

ISPH Modelling of Rayleigh-Taylor Instability

Mostafa Safdari Shadloo

Faculty of Engineering and Natural Sciences,
Advanced Composites and Polymer Processing Laboratory
Sabanci University,
Istanbul, Turkey
mostafa@sabanciuniv.edu

Mehmet Yildiz

Faculty of Engineering and Natural Sciences,
Advanced Composites and Polymer Processing Laboratory
Sabanci University,
Istanbul, Turkey
meyildiz@sabanciuniv.edu

Abstract- This paper presents a *Smoothed Particle Hydrodynamics (SPH)* solution to a *Rayleigh-Taylor Instability (RTI)* problem in an incompressible viscous two-phase immiscible fluid with an interfacial tension. The evolution of the fluid-fluid interface is numerically investigated for four different density ratios. The simulation outcomes are compared with existing results in literature. Three stages of instability, namely the exponential growth rate, the formation of circular form at the crest of spike and the appearance of the final shape of instability, are discussed for different density ratios. It is shown that the numerical algorithm used in this work is capable of capturing the complete physics behind the RTI, such as interface evolution, growth rate and secondary instability accurately, and successfully.

I. INTRODUCTION

Instability at the interface between two horizontal parallel fluids of different viscosities and densities with the heavier fluid at the top and the lighter at the bottom is known as the Rayleigh–Taylor Instability (RTI) to honour the pioneering works of Lord Rayleigh [1] and G. I. Taylor [2]. This phenomenon can be observed in a wide range of natural and astrophysical events. The instability initiates when a multiphase fluid system with different densities experiences gravitational force. As a result, an unstable disturbance tends to grow in the direction of the gravitational field, thereby releasing the potential energy of the system and reducing the combined potential energy of the fluids. Due to being an important phenomenon in many fields of engineering and sciences, the RTI has been widely investigated by using experimental [3, 4], analytical [5, 6] as well as numerical approaches [7, 8].

The Smoothed Particle Hydrodynamics (SPH) is a relatively new numerical approach that has attracted significant attention in the last 15 years. Compared with the conventional mesh-dependent computational fluid dynamics (CFD), the SPH method exhibits unique advantages in modelling fluid flows and associated transport phenomena due to its capabilities of handling complex material surface behaviour as well as modelling complicated physics in a relatively simple manner.

There are a few works which have used the SPH method to model the RTI problem [12-15]. Cummins and Rudman [9] solved the RTI phenomenon using a projection method-

based Incompressible SPH (ISPH) approach. Tartakovsky et al. [10] modelled the Rayleigh-Taylor instability in a multiphase and multi-component mixture with the Weakly Compressible SPH (WCSPH) method through solving momentum balance and species mass balance equations concurrently. Hu and Adams [11] solved the RTI problem as a benchmarking problem through combining projection methods used in [9] and [12]. More recently Grenier et al. [13] presented a WCSPH formulation for simulating interface flows, and model the RTI to validate their numerical scheme. It should be emphasized here that none of these cited works has included the effect of the surface tension in their simulations. These works handled the RTI as a validation test case for their algorithm and did not focus on the physics of the problem in detail.

The aim of this work is to simulate the RTI by using the ISPH method, thereby showing the ability of the SPH technique to capture this hydrodynamic instability and relevant physics for a wide range of density ratios. The current presentation differs from earlier works in the following aspects: Even though multiphase grid-based methods considered the RTI problem in detail, it has been barely considered within the context of the SPH method, and if so, mainly for the density ratio of $\rho_2 / \rho_1 = 1.8$.

II. SMOOTHED PARTICLE HYDRODYNAMICS

A. Introduction

Initially developed to solve the astrophysics problems in 1977 by Gingold and Monaghan, and Lucy in separate works [14, 15], and later extended to solve a wide variety of fluid dynamics problems [16-18], SPH is a member of Lagrangian methods. The SPH method is based on the smoothing of the hydrodynamics properties of fluid elements, which are represented by movable points (also referred to as particles), over the solution domain using a weighting function, $W(r_{ij}, h)$, or in short W_{ij} . The weighting function W_{ij} (also known as the kernel function in the SPH literature) is an arbitrary function (e.g. exponential, spline, and etc.) with some special properties as listed [19]. Here, r_{ij} is the magnitude of the distance vector ($\vec{r}_{ij} = \vec{r}_i - \vec{r}_j$) between the particle of interest i and its

neighbour \mathbf{j} , $\bar{\mathbf{r}}_i$ is the position vector defining the center point of the kernel function and h defines the support domain's length of the particle of interest.

The integral estimate or the kernel approximation to an arbitrary function $f(\bar{\mathbf{r}}_i)$ or briefly f_i can be introduced as

$$f_i \equiv \langle f_i \rangle \equiv \int_{\Omega} f_j W_{ij} d^3 \bar{\mathbf{r}}_j. \quad (1)$$

Replacing the integration in Eq. (1) with SPH summation over particle \mathbf{j} and setting the infinitesimal volume element $d^3 \bar{\mathbf{r}}_j$ to the inverse of the number density $1/\psi_j$, one can write the SPH interpolation for any arbitrary field f_i as.

$$f_i = \sum_j f_j W_{ij} / \psi_j, \quad (2)$$

where the number density ψ_i for the particle \mathbf{i} is defined as

$$\psi_i = \sum_j W_{ij}, \quad (3)$$

which is also equal to $\psi_i = \rho_i / m_i$.

The SPH approximation for the gradient of the arbitrary function f_i can be introduced as

$$\frac{\partial f_i}{\partial x_i^k} = \sum_j \frac{f_j}{\psi_j} \frac{\partial W_{ij}}{\partial x_i^k}. \quad (4)$$

An alternative and more accurate SPH approximation for the gradient of a vector-valued function in the form of the SPH interpolation can be introduced as

$$\frac{\partial f_i^p}{\partial x_i^k} a_{ij}^{ks} = \sum_j \frac{(f_j^p - f_i^p)}{\psi_j} \frac{\partial W_{ij}}{\partial x_i^s}, \quad (5)$$

where $a_{ij}^{ks} = \sum_j (r_{ji}^k / \psi_j) (\partial W_{ij} / \partial x_i^s)$ is a corrective second-rank tensor. This form is referred to as the corrective SPH gradient formulation that can be used to eliminate particle inconsistencies. It should be noted that the corrective term a_{ij}^{ks} is ideally equal to Kronecker delta δ^{ks} for a continuous function.

There are also different ways to approximate the second-order derivative within the context of SPH [16]. Throughout this work, all modeling results are obtained with the usage of following corrective spatial second-order SPH discretization schemes

$$\frac{\partial^2 f^p(\bar{\mathbf{r}}_i)}{\partial x_i^k \partial x_i^k} a_{ij}^{pm} = 8 \sum_j \frac{1}{\psi_j} (f_i^p - f_j^p) \frac{r_{ij}^p}{r_{ij}^2} \frac{\partial W_{ij}}{\partial x_i^m}, \quad (6)$$

$$\frac{\partial^2 f_i^p}{\partial x_i^k \partial x_i^k} (2 + a_{ij}^m) = 8 \sum_j \frac{1}{\psi_j} (f_i^p - f_j^p) \frac{r_{ij}^s}{r_{ij}^2} \frac{\partial W_{ij}}{\partial x_i^s}. \quad (7)$$

Since the former one is only valid for divergence free vector-valued functions, throughout this work, it is used for the Laplacian of the velocity, whereas the later one is used for the Laplacian of the pressure in the pressure Poisson equation.

Finally in the present simulations, the compactly supported two-dimensional quintic spline is used.

$$W(r_{ij}, h) = \alpha \begin{cases} (3 - s_{ij})^5 - 6(2 - s_{ij})^5 + 15(1 - s_{ij})^5 & \text{if } 0 \leq s_{ij} < 1 \\ (3 - s_{ij})^5 - 6(2 - s_{ij})^5 & \text{if } 1 \leq s_{ij} < 2 \\ (3 - s_{ij})^5 & \text{if } 2 \leq s_{ij} \leq 3 \\ 0 & \text{if } s_{ij} \geq 3 \end{cases}. \quad (8)$$

Here, $s_{ij} = r_{ij} / h$ and the spline coefficient α is equal to $7/478\pi h^2$ for 2-D quintic spline.

B. Governing equations

We consider incompressible immiscible two phase Newtonian fluids. The motions of such fluids are governed by the conservation of mass and momentum equations, which are respectively given in the Lagrangian form as

$$D\rho / Dt = -\rho \nabla \cdot \bar{\mathbf{v}}, \quad (9)$$

$$\rho D\bar{\mathbf{v}} / Dt = \nabla \cdot \underline{\underline{\boldsymbol{\sigma}}} + \bar{\mathbf{f}}^s + \rho \bar{\mathbf{g}}, \quad (10)$$

where $\bar{\mathbf{v}}$ is the fluid velocity vector, ρ is the fluid density, $\underline{\underline{\boldsymbol{\sigma}}}$ is the total stress tensor, $\bar{\mathbf{g}}$ is gravitational force, and $\bar{\mathbf{f}}^s$ is the surface tension force. The total stress is defined as, $\underline{\underline{\boldsymbol{\sigma}}} = -p \underline{\underline{\mathbf{I}}} + \underline{\underline{\mathbf{T}}}$ where p is the absolute pressure, $\underline{\underline{\mathbf{I}}}$ is the identity tensor, and $\underline{\underline{\mathbf{T}}} = \mu (\nabla \bar{\mathbf{v}} + (\nabla \bar{\mathbf{v}})^T)$ is the viscous part of the total stress tensor, where μ is the dynamic viscosity. Finally, D / Dt is the material time derivative operator.

C. Computation of the surface tension force

The surface tension force is modelled using the Continuum Surface Force (CSF) approach where the interfacial force is only supported at the fluid-fluid interface with finite thickness, and is absent in the bulk. Here, it is assumed that the surface tension coefficient σ is constant. In the CSF model [20], the surface tension force per unit volume $\bar{\mathbf{f}}^s$ is defined as

$$\bar{\mathbf{f}}^s = \sigma \kappa \bar{\mathbf{n}} \delta^s, \quad (11)$$

where $\bar{\mathbf{n}}$ is the unit normal vector to the interface, κ is the curvature of the interface and δ^s is a normalized surface delta function.

We assign colour values $C = 0$ and $C = 1$ to all particles to differentiate between phase 1 and phase 2, respectively. On the interface, we smooth the colour function by

$$C_i = \sum_j W_{ij} C_j / \sum_j W_{ij}. \quad (12)$$

Then the unit normal $\bar{\mathbf{n}}$ is computed by

$$\bar{\mathbf{n}} = \nabla C / |\nabla C|. \quad (13)$$

Further the curvature is calculated using

$$\kappa = -\nabla \cdot \bar{\mathbf{n}}. \quad (14)$$

There are many possible choices for δ^s , but in practice, it is often approximated as $\delta^s \approx |\nabla C|$ [21].

D. Numerical scheme

For the time marching in the ISPH approach, we have used a first-order Euler time step scheme. Hence, particles are moved from their current positions $\bar{\mathbf{r}}_i^{(n)}$ with their current velocities $\bar{\mathbf{v}}_i^{(n)}$ at time t^n to their new estimated positions at $\bar{\mathbf{r}}_i^*$ at time $t^n + \Delta t$, which is given by

$$\bar{\mathbf{r}}_i^* = \bar{\mathbf{r}}_i^{(n)} + \bar{\mathbf{v}}_i^{(n)} \Delta t. \quad (15)$$

Afterwards, the intermediate velocities $\bar{\mathbf{v}}_i^*$ are computed on these temporary particle locations through the solution of the momentum balance equations with forward time integration by omitting the pressure gradient term as

$$\bar{\mathbf{v}}_i^* = \bar{\mathbf{v}}_i^{(n)} + \bar{\mathbf{f}}_i^{(n)} \Delta t. \quad (16)$$

Then, at the correction step, we correct $\bar{\mathbf{v}}_i^*$ by solving the equation

$$\bar{\mathbf{v}}^{(n+1)} = \bar{\mathbf{v}}^* - (\Delta t / \rho) \nabla p^{(n+1)}, \quad (17)$$

with the incompressibility constraint of $\nabla \cdot \bar{\mathbf{v}}^{(n+1)} = 0$.

The divergence of Eq. (17) leads to the pressure Poisson equation as

$$\nabla \cdot \bar{\mathbf{v}}^* / \Delta t = \nabla \cdot (\nabla p / \rho). \quad (18)$$

The boundary condition for the pressure is obtained by projecting Eq. (18) on the outward unit normal vector $\bar{\mathbf{n}}$ to the boundary. Thus, we obtain the Neumann boundary condition

$$(\rho / \Delta t) \bar{\mathbf{v}}^* \cdot \bar{\mathbf{n}} = \nabla p \cdot \bar{\mathbf{n}}. \quad (19)$$

For stationary no-slip walls, Eq. (19) takes the form of the Neumann boundary condition, $\nabla p \cdot \bar{\mathbf{n}}$. Finally, with the correct velocity field for $t^{(n+1)}$, all fluid particles are advected to their new positions $\bar{\mathbf{r}}_i^{(n+1)}$ using an average of the previous and current particle velocities as

$$\bar{\mathbf{r}}_i^{(n+1)} = \bar{\mathbf{r}}_i^{(n)} + 0.5 (\bar{\mathbf{v}}_i^{(n)} + \bar{\mathbf{v}}_i^{(n+1)}) \Delta t. \quad (20)$$

To enhance the robustness of the model, and circumvent the particle disorderness and fracture induced numerical problems, artificial particle displacement approach is used in advecting particle positions [16].

III. DEFINITION OF PROBLEM

The RTI can occur in a multiphase fluid system where a layer of heavy fluid is placed on top of another layer of light fluid with an interface having a small initial perturbation. This disturbance will grow to produce spikes of heavy fluids moving downward into the lighter fluid, and bubbles of the lighter fluid moving upward. For modeling the RTI phenomena, a rectangular computational domain with the dimensions of $[0, H] \times [0, 2H]$ is used. For simplicity, H is chosen to be unity ($H=1m$). The number of particles for each fluid region is the same. An initial sinusoidal perturbation is applied to the fluid–fluid interface through swapping the colour fields of particles in the vicinity of the perturbation. The magnitude of the perturbation is $(\zeta_0/H \approx 0.05)$, where ζ_0 is the initial amplitude of the applied disturbance. In all simulations, solid boundaries are treated using Multiple Boundary Tangents (MBT) method [22], and the no-slip boundary conditions are imposed on the solid boundaries.

To be able to show the effect of density on the RTI, we have conducted simulations for several density ratios, ρ_2 / ρ_1 , where the density of the lower fluid layer is set to be $\rho_1 = 1000 \text{ (kg/m}^3\text{)}$, unless stated otherwise. When all modelling parameters are active, the surface tension force per unit length (σ) acts only on the interface particles in the unit normal direction, while the gravity (g) acts in downward direction on all particles. Also, to be able to show the effect of Bond number, Bo , on the RT instability we have kept the value of gravity constant ($g=0.09 \text{ m/s}^2$) and changed the surface tension coefficient accordingly. The Bond number is a dimensionless number that reveals the importance of surface tension forces compared to body forces, and is defined as $Bo = \Delta \rho g l^2 / \sigma$ where l is the characteristic length scale, which is taken as the width of the

domain, $l = H$ in this work, and $\Delta\rho = \rho_2 - \rho_1$. A high Bo number indicates that the surface tension has less influence in the flow system, while a low Bo number indicates that surface tension dominates.

IV. VALIDATION AND CONVERGENCE

In order to demonstrate convergence, we have conducted numerical simulations with three different particle resolutions, namely, 60×120 , 100×200 and 200×400 . Fig. 1 shows the interface shape for these simulations at $t(g/H)^{0.5} = 5.0$ for the Reynolds number of ($Re=420$) where $Re = \rho_2 \sqrt{gH^3} / \mu_2$. In these simulations, the initial fluid-fluid interface is disturbed using the relation $y = 1 - 0.15 \sin(2\pi x)$ and the two-phase fluid system has density and viscosity ratios of $\rho_2 / \rho_1 = 1.8$ ($\rho_1 = 1 \text{ kg/m}^3$) and $\mu_2 / \mu_1 = 1.8$ ($\mu_1 = 1 \text{ Pas}$), respectively.

For the long term time evolution of the instability, one can notice that the solution has converged. However, the particle resolution of 60×120 is insufficient to capture the development of small scale structures, namely the secondary instability, in the outer core region of the roll-up (in particular, see the top-left side of Fig.1). Nevertheless, one can still see the inception of this secondary instability at the interface. As for the particle resolution of 100×200 , the number of particles is sufficient to predict this secondary roll-up at the fluid-fluid interface. Finally, at 200×400 , the particle resolution is fine enough to be able produce all these small scale phenomena and to capture sharp curved interfaces in the solution domain. Since the investigation of these small scale secondary instabilities is not the focus of our current presentation, in the rest of the paper, the particle resolution of 100×200 is used to simulate the RTI problem.

Furthermore, we have shown in Fig. 2 that even with low particle resolution (60×120), the ISPH model employed in this work can produce a result which is in a good agreement with that of Level Set reported in [13, 23]. This can be attributed to the faster convergence rate of the SPH method than the Level set method. One should also notice from Fig. 2 that unlike the WCSPH approach [13], the ISPH method can capture the onset of the secondary instability without necessitating the usage of high particle resolution. It should also be noted that the current ISPH treatment of the RTI problem captures the strong roll-up in the core region of the instability, hence implying that the model does not suffer from the artificial surface tension effect [18].

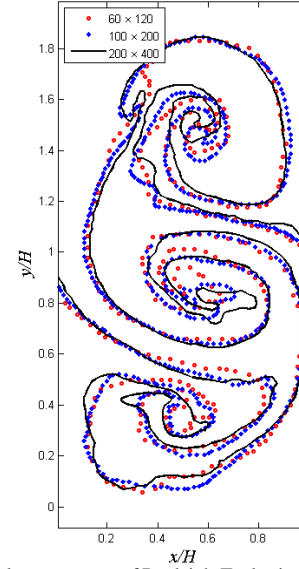


Figure 1. Spatial convergence of Rayleigh-Taylor instability using three different particle resolution, namely, 60×120 , 100×200 and 200×400 at

$$t(g/H)^{0.5} = 5.0$$

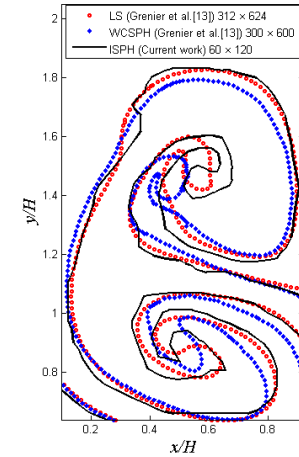


Figure 2. The comparison of ISPH solutions for Rayleigh-Taylor instability with WCSPH and LS reported in [13].

V. RESULTS

To illustrate the influence of density ratio on the RTI, in Fig.3, we present the sequence of the evolution of the interface for the density ratios of $\rho_2 / \rho_1 = 2, 5$ and 100 , respectively at the Reynolds number of 300 and the Bond number of 100 , where the left half of each subfigures shows the particle distribution, whereas the right half presents the pressure contours.

There are three apparent stages in the development of the instability. The first stage corresponds to earlier times in

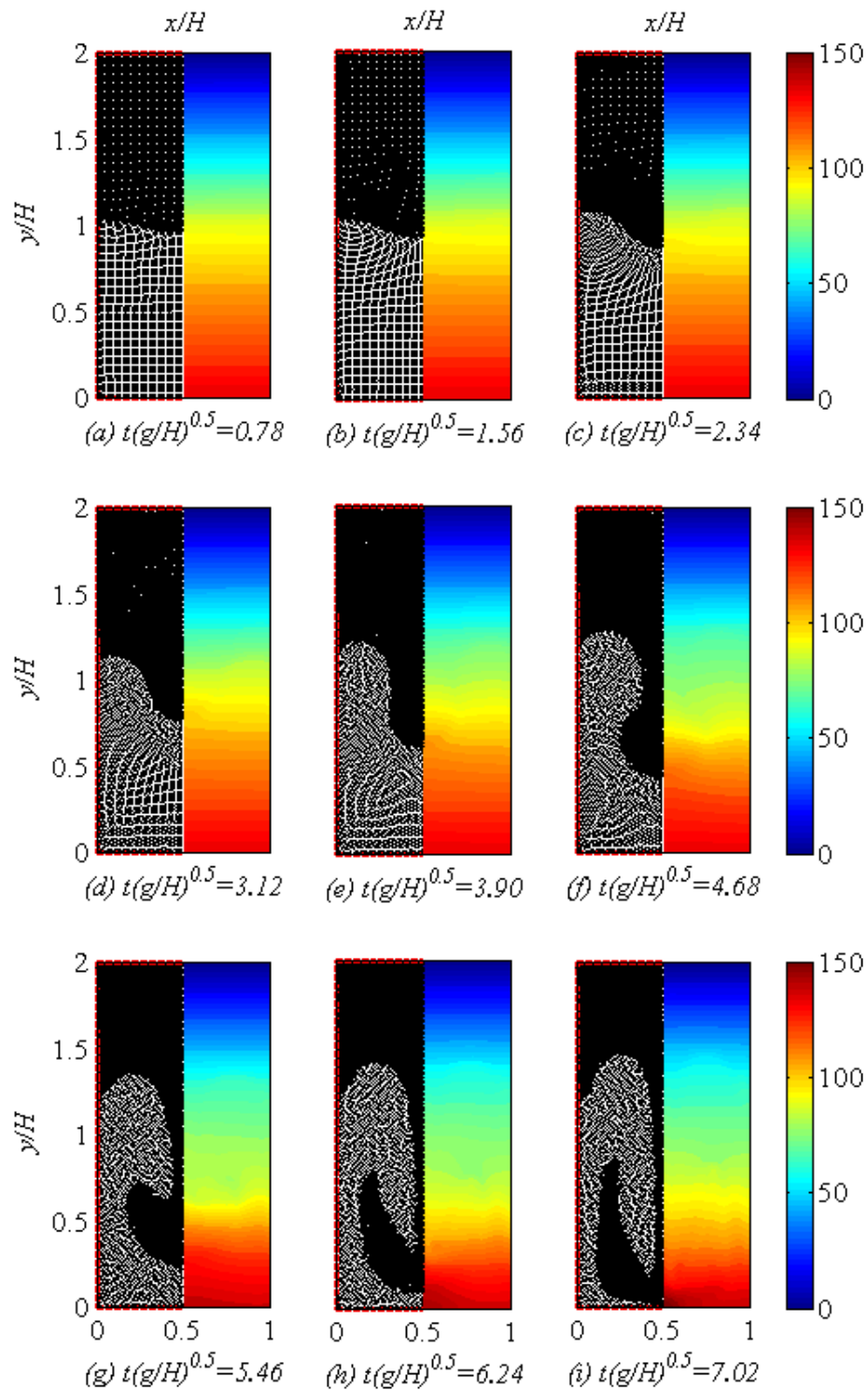


Figure 3. The sequence of the evolution of the interface from a single mode perturbation for density ratio of $\rho_2/\rho_1=2$ at the Reynolds number, of 300 and the Bond number of 100, where the left half of each subfigures shows the particle distribution, whereas the right half presents the pressure contours.

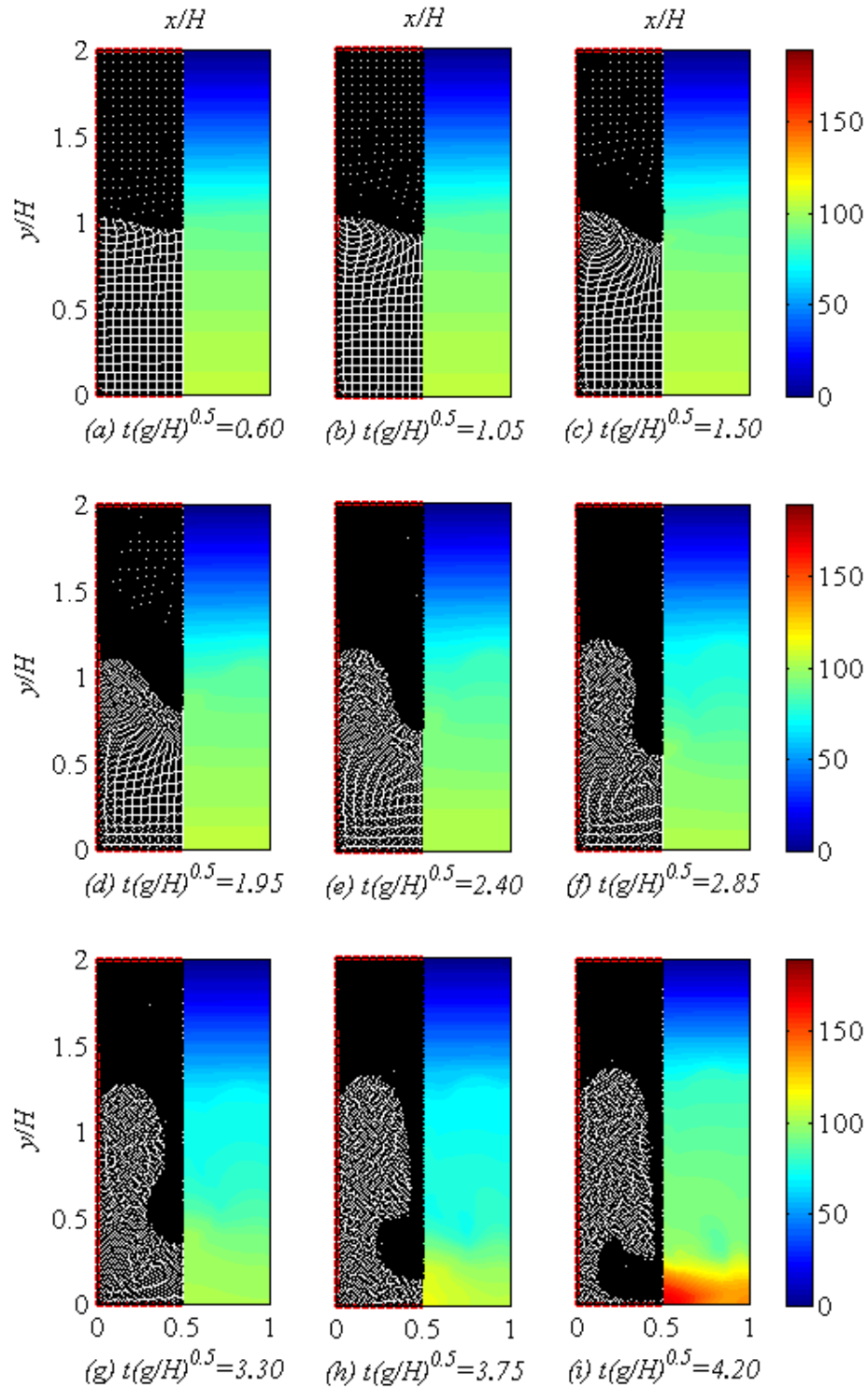


Figure 4. The sequence of the evolution of the interface from a single mode perturbation for density ratio of $\rho_2 / \rho_1 = 5$ at the Reynolds number of 300 and the Bond number of 100, where the left half of each subfigures shows the particle distribution, whereas the right half presents the pressure contours.

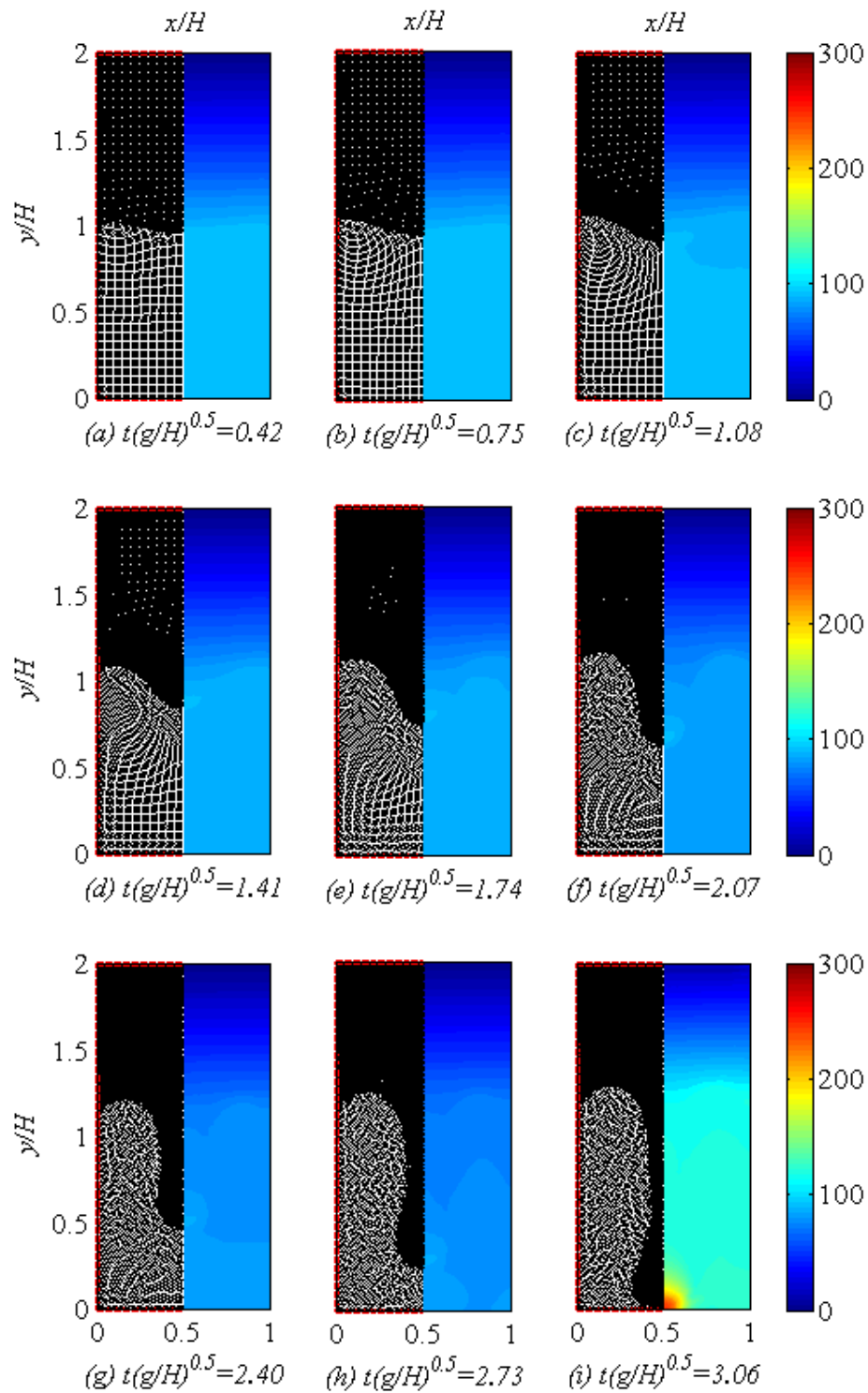


Figure 5. The sequence of the evolution of the interface from a single mode perturbation for density ratio of $\rho_i / \rho_l = 100$ at the Reynolds number of 300 and the Bond number of 100, where the left half of each subfigures shows the particle distribution, whereas the right half presents the pressure contours.

simulations where the initial disturbance grows exponentially, and the fluid layers retain their initial sinusoidal shape as can be seen from the first row of Figs.3 through 5. At this stage, the shape of the RTI instability is the same for all density ratios albeit the differences in the growth rate. The growth rate increases with increasing density ratio. At the second stage, the leading spikes supported by a column of heavier fluids (so-called stem) develop and circular shapes on the crest of the spike appear (see the second row of Figs.3 through 5). It should be observed that, for lower density ratios, the stem is wider and the circular tip of the stem has a larger radius.

The last stage corresponds to the formation of the final shape of the instability before its impact on the stationary wall. At this stage, the stem elongates and gets thinner, and the lighter fluid is entrained into the circular drop at the trough of the spike. The instability has different patterns for different density ratios. For a lower density ratio, the crest of the spike acquires a mushroom cap shape. It is noted that the entrainment of the lighter fluid leads to thinner trough for the lower density ratios; however for the higher density ratios the stem has approximately uniform width during its elongation and the spike conserves its circular shape (see the last row of Figs.3 through 5). It is worthy of mentioning that for higher density ratios, namely $\rho_2 / \rho_1 > 10$, the dramatic differences in the shape of spike and bubble become less pronounced. Density ratio affects the growth rate of the instability. However, the transient and final shapes of the instability are rather independent of the density ratio.

It should be further noted that as the density ratio increases, the pressure at the tip of the spike gets greater. This can be explained considering the potential energy of the fluid. The heavier the fluid, the higher its initial potential energy is. This potential energy is converted to the kinetic energy as the instability grows. In time, the fluid jet slows down as it approaches to the bottom stationary wall. Upon the impact on the wall, the spike feels higher pressure region at its crest due to the deceleration of fluid jet.

VI. CONCLUSION

Under the assumption of 2D incompressible immiscible two-phase viscous flow, a parametric investigation of the Rayleigh-Taylor instability of a fluid layer resting on the second lighter fluid was performed. Having tested the spatial convergence, and validated the model with results available in the literature, we investigated the effect of density ratio on the RT instability. It was numerically illustrated that the density ratio has a significant effect on the evolution and the final shape of the instability.

ACKNOWLEDGMENTS

Funding provided by the European Commission Research Directorate General under Marie Curie International Reintegration Grant program with the Grant Agreement number of 231048 (PIRG03-GA-2008-231048) is gratefully acknowledged.

REFERENCES

- [1] Lord Rayleigh, Investigation of the character of the equilibrium of an incompressible heavy fluid of variable density. Proceedings of the London Mathematical Society, 14(1883) 170-177.
- [2] G.I. Taylor, The instability of liquid surfaces when accelerated in a direction perpendicular to their planes. Proceedings of the Royal Society of London, A 201(1950) 192-196.
- [3] J. T. Waddell, C. E. Niederhaus, J. W. Jacobs, Experimental study of Rayleigh–Taylor instability: Low Atwood number liquid systems with single-mode initial perturbations, Physics of Fluids, Volume 13, Issue 5, pp. 1263-1273 (2001).
- [4] M. J. Andrews, S. B. Dalziel, Small Atwood number Rayleigh–Taylor experiments, Phil. Trans. R. Soc. A (2010) 368, 1663–1679.
- [5] K. O. Mikaelian, “Effect of viscosity on Rayleigh–Taylor and Richtmyer–Meshkov instabilities,” Phys. Rev. E 47 (1993) 375–383.
- [6] A. R. Piriz, O. D. Cortázar, J. J. López Cela, N. A. Tahir, The Rayleigh–Taylor instability, Am. J. Phys. 74 (12) (2006) 1095-1098.
- [7] D. I. Pullin, Numerical studies of surface-tension effects in nonlinear Kelvin–Helmholtz and Rayleigh–Taylor instability, J. Fluid Mech. 119 (1982) 507-532.
- [8] D. L. Youngs, “Numerical simulation of turbulent mixing by Rayleigh–Taylor instability,” Physica D 12 (1984) 32-44.
- [9] S. J. Cummins, M. Rudman, An SPH Projection Method, J. Comput. Phys. 152(1999), 584–607.
- [10] A.M. Tartakovsky and P. Meakin, A smoothed particle hydrodynamics model for miscible flow in three-dimensional fractures and the two-dimensional Rayleigh Taylor instability, J. Comput. Phys. 207 (2) (2005), pp. 610–624.
- [11] X. Y. Hu, N.A. Adams, An incompressible multi-phase SPH method, J. Comput. Phys. 227 (2007) 264–278.
- [12] S. Shao, E. Y.M. Lo, Incompressible SPH method for simulating Newtonian and non-Newtonian flows with a free surface, Advances in Water Resources 26 (2003) 787–800.
- [13] N. Greniera, M. Antuonob, A. Colagrossib, D. Le Touzéa and B. Alessandrini, An Hamiltonian interface SPH formulation for multi-fluid and free surface flows, J. Comput. Phys. 228(22)(2009) 8380–8393.
- [14] R.A. Gingold, J.J. Monaghan, Smooth Particle Hydrodynamics: theory and application to non spherical stars, Mon. Not. R. Astron. Soc. 181 (1977) 375.
- [15] L.B. Lucy, A Numerical Approach to the Testing of the Fission Hypothesis, Astro. J. 82 (1977) 1013.
- [16] M. S. Shadloo, A. Zainali, S. H. Sadek, M. Yildiz, “Improved Incompressible Smoothed Particle Hydrodynamics Method for Simulating Flow around Bluff Bodies”, Comput. Methods Appl. Mech. Engrg. 200 (2011) 1008–1020.
- [17] J. J. Monaghan, Simulating free surface flows with sph. Journal of Computational Physics 110(1994)399–406.
- [18] M. S. Shadloo, M. Yildiz, “Numerical modeling of Kelvin–Helmholtz Instability Using Smoothed Particle Hydrodynamics Method”, Int. J. Numer. Methods Engrg., DOI: 10.1002/nme.3149.
- [19] J.J. Monaghan, Smoothed particle hydrodynamics, Rep. Prog. Phys. 68 (2005), p. 1703.
- [20] J. U. Brackbill, D. B. Kothe, C. Zemach, A continuum method for modelling surface tension. Journal of Computational Physics 100 (1992) 335–354.
- [21] Morris JP. Simulating surface tension with smoothed particle hydrodynamics. Int. J. Numer. Methods Fluids 33(3) (2000)333–353.
- [22] M. Yildiz, R.A. Rook and A. Suleman, SPH with the multiple boundary tangent method, Int. J. Numer. Methods Engrg. 77 (10) (2009), 1416–1438.
- [23] G. Colicchio, Violent disturbance and fragmentation of free surfaces, Ph.D. Thesis, University of Southampton, UK, 2004.